Resonant light transport through Mie modes in photonic glasses

P. D. García,[1,*] R. Sapienza,[1] J. Bertolotti,[2] M. D. Martín,[3] Á Blanco,[1] A. Altube,[1] L. Viña,[3] D. S. Wiersma,[2] and C. López[1]

[1]*Instituto de Ciencia de Materiales de Madrid (CSIC) and Unidad Asociada CSIC-UVigo, Cantoblanco 28049 Madrid, Spain*

[2]*European Laboratory for Nonlinear Spectroscopy & INFM-BEC, 50019 Sesto Fiorentino (Florence), Italy*

[3]*Departamento de Fisica de Materiales, Universidad Autonoma de Madrid, Cantoblanco 28049 Madrid, Spain*

(Received 8 April 2008; published 13 August 2008)

We present an optical characterization of photonic glasses, composed of randomly arranged, monodisperse dielectric spheres packed at high filling fractions. We provide a detailed optical study of the resonant behavior of diffuse light transport through such systems. By means of independent static and dynamic measurements, we show resonances in the transport mean free path, diffusion constant, and also energy velocity of light. We also show that the main transport parameters can be controlled by varying the sphere diameter.

DOI: 10.1103/PhysRevA.78.023823 PACS number(s): 42.25.Dd, 42.25.Bs

I. INTRODUCTION

The control of light transport is crucial to design and tailor new photonic devices with increased optical performance in the same manner as controlling electron transport is at the basis of semiconductor and electronic technology. In recent years, a new frontier has emerged, with the goal of controlling light propagation through interference in artificially engineered optical materials and metamaterials. Extraordinary progress has been made in the fabrication of nanophotonic structures, with many novel optical properties [1]. While (ordered) periodic photonic media, i.e., photonic crystals, take advantage of the periodicity in the dielectric constant and the consequent long-range correlation to mold the flow of light [2,3], disordered ones, with no positional order, can still strongly affect light transport [1,4–6] and, for example, in the presence of short-range correlation, exhibit band-gap-like effects [7]. Conventional nonabsorbing materials are homogeneous and nondispersive, i.e., they are clear and transparent, and phase and energy travel with the same velocity. Optical propagation is then determined by the shape of the interfaces between various such materials (e.g., a curve surface boundary acts as a lens). If the material is absorptive, dispersion is introduced (brought about by the Kramers-Kronig relations) whereby the phase velocity loses most of its usefulness, and group velocity (at which pulses travel) takes over to describe the transport of energy. In contrast, nonabsorbing but nanostructured materials can create a new class of systems in which the dispersion is controlled via light interference. Photonic band-gap materials, for instance, are systems where extinction is built up from multiple interference (Bragg reflection) creating a region of extinction and anomalous dispersion. In this way, the relevant velocities can be engineered, for instance, to create devices for dispersion compensation. An entirely new scenario is presented when disorder is added to the mixture.

Usually, disordered media are opaque and white, i.e., nondispersive. In such a disordered medium, the group velocity can only be associated with the ballistic (or unscattered) component, and therefore cannot be applied to describe the transport of energy, which, for large enough optical thicknesses, is governed by the scattered light.

When this regime of diffusive propagation is set up, not only phase but also group velocity fail to give an account of light transport, and a new quantity describing the transport of energy in the new diffusive regime is required. The velocity of the scattered light propagation inside disordered media needs to be defined by the velocity of the transported energy and is given by the ratio of the energy flux to the energy density in any point of the sample. This, in general, is very complex and given neither by the group velocity nor the phase velocity [8,9]. The energy velocity can be drastically altered (reduced) in the presence of scattering resonances: in an extreme case of light diffusion in a cold atomic cloud, the atomic energy spectrum can be so resonant to the incident light that the energy velocity can be as low as a few thousand meters per second ($v_e/c \sim 10^{-5}$) [10].

Disordered materials are composed basically by oxides or semiconductor powders [11,12], random solid distributions of polydisperse spheres [13,14], nanostructured semiconductors such as porous GaP [15], or by colloidal suspensions of polymer spheres [7]. In ordinary disordered materials, like a semiconductor powder, the individual modes of each building block are usually neglected and a homogeneous distribution of light, in wave vector and frequency, is assumed [1]. In contrast, a single dielectric sphere with size comparable to the wavelength of light can sustain electromagnetic resonances, called Mie modes [16]. Figure 1 shows two different modes in a dielectric sphere at two different energies [17]. These resonant electromagnetic modes in dielectric spheres are analogous to electronic orbitals in atoms [18]. In this work, we present a detailed characterization of the resonant behavior of light transport through a resonant random material we recently proposed and dubbed "*photonic glass*" (PG) [19,20]. The main property of this new system compared with other commonly used disordered materials is the monodispersity of its constituents (Fig. 2). We discuss the properties of light diffusion through such a system and present the optical characterization by means of static and dynamic measurements. With an optical characterization of the system, we also point out that light transport can be controlled by chang-

*Author to whom correspondence should be addressed. dgarcia@icmm.csic.es

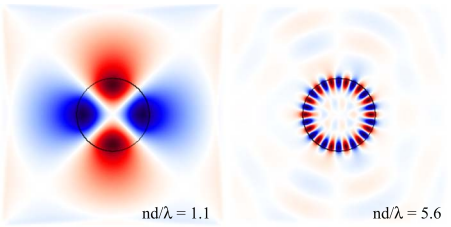

FIG. 1. (Color online) Modulus of the scattered field for a sphere diameter $d=1100$ nm and refractive index $n=3.4$ in the case of low ($d/\lambda=0.33$) and high energy ($d/\lambda=1.65$). The confinement of the mode is proportional to the Q factor of the spheres, which increases with the field energy.

ing sphere diameter. In the final part of the paper, an estimation of the energy velocity in the system and different theoretical approximations are also discussed.

II. PHOTONIC GLASSES PREPARATION

It is well known that submicrometer dielectric spheres are able to self-assemble forming fcc structures, which are commonly called synthetic opals. These structures have been widely used to study the properties of photonic crystals.

A synthetic opal is usually grown placing a clean microslide vertically in a vial containing an aqueous dilute colloidal suspension of spheres [21]. Charge interaction between the spheres allows them to self-assemble. The modeling of the two-body sphere-sphere potential of an aqueous colloidal suspension represents a very complicated problem [22] that can be approximated as a sum of two terms: $U(r)=\phi(r)+U_{\mathrm{vdW}}(r)$, where $\phi(r)$ is the electrostatic repulsive potential due to the sphere surface charge and $U_{\mathrm{vdW}}(r)$ is the attractive van de Waals potential. We have developed a method based on this two-body interaction between the spheres to grow completely disordered arrangements of monodisperse ($<2\%$) dielectric spheres. This new three-dimensional system constitutes a novel random material for light: photonic glass [19,20]. The picture in the upper panel of Fig. 3 shows an opal-based photonic crystal (with visible iridescences related to Bragg reflections) and a photonic glass (white surface), both grown from polystyrene (PS) spheres with $d=1100$ nm, where d is the sphere diameter. The lower panel shows scanning electron microscopy (SEM) images of the corresponding systems. Photonic glasses can be grown very uniform, with areas of a few square millimeters and thicknesses of some hundreds of micrometers. The growth procedure consists in adding extra charge (electrolytes) to the initial (extra charge-free) colloidal suspension, which attenuates the surface sphere charge and, therefore, $\phi(r)$. Figure 4 shows the total interaction potential, $U(r)$, between spheres as a function of salt concentration (thus of the extra charge concentration). The calculation of this interaction is based on the solution proposed in Ref. [22]. Extra electrolytes (ions) can be produced by adding salts (which dissociate producing ions in dissolution) or acids (which also dissociate producing protons).

The attenuation of the repulsive potential gives rise to a net attractive potential between spheres. In this case, the

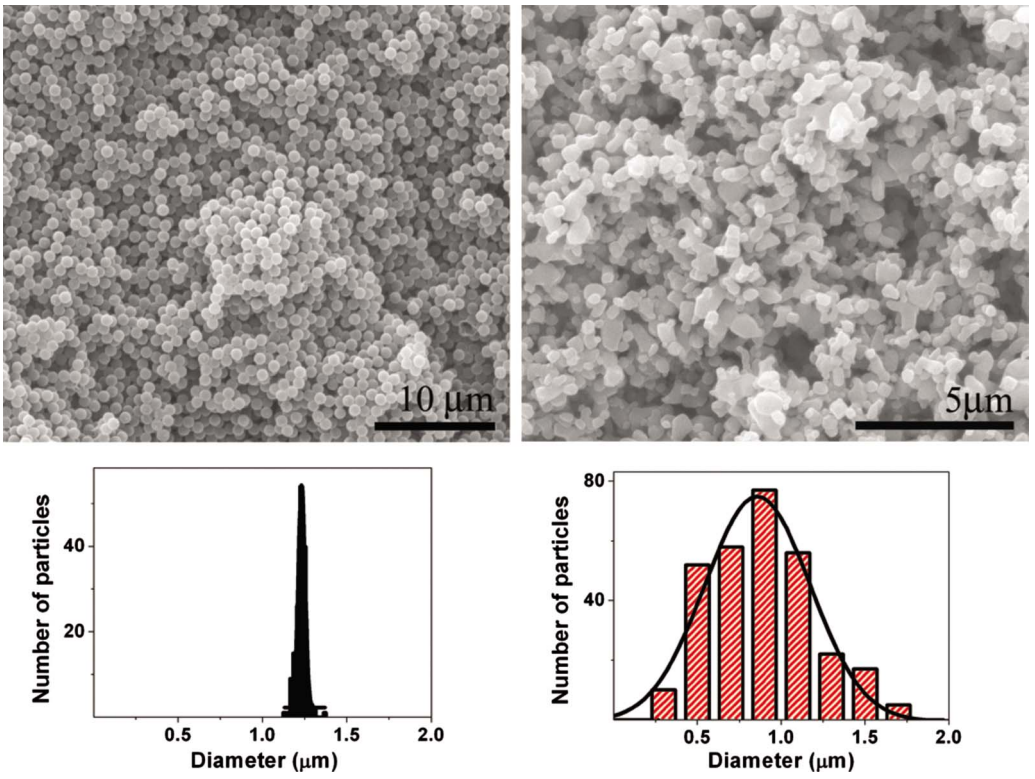

FIG. 2. (Color online) Top: (Left) Scanning electron microscopy (SEM) image from the photonic glass surface composed of polystyrene (PS) spheres with a diameter of 1200 nm. (Right) SEM image from TiO_2 powder surface with an average particle diameter 850 nm. Bottom: Corresponding histogram of particle sizes from the photonic glass (left) and TiO_2 powder (right).

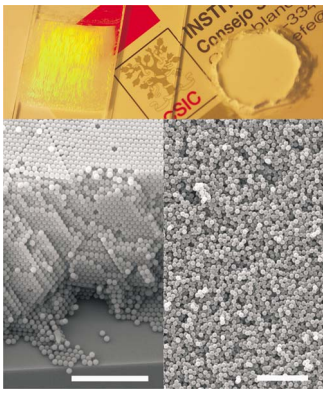

FIG. 3. (Color online) Top: picture shows an opal-based photonic crystal (left) which shows visible iridescences due to Bragg reflections and a photonic glass (right) white and without any trace of Bragg features. Bottom: (Left) SEM image from a photonic crystal cleaved edge (scale bar is 10 μm). (Right) SEM image from a photonic glass surface (scale bar is 10 μm). Both samples are made of PS spheres (2% of polidispersity measured by TEM) and have centimeters squared areas and millimeters thickness.

number of effective collisions between spheres increases and clusters are formed by flocculation in the suspension. The number of effective collisions that give rise to sphere coagulation grows due to the total potential attenuation. Then, cluster size also grows with electrolyte concentration. With the sedimentation of these clusters, a random arrangement of spheres is formed. Lowering the repulsive potential, the size of the clusters formed by flocculation is increased. The size of these clusters has an important effect on the filling fraction (ff) [23] of the system and strongly affects the physical parameters that describe light transport. Photonic glasses grown from bigger clusters present a lower filling fraction because the interclusters volume is empty. Changing the salt concentration, we can grow PG with different ff. Figure 5 shows the average ff from different photonic glasses as a function of the salt concentration (electrolyte concentration) from 0.74 (the expected theoretical volume for a perfect fcc structure) to 0.55. These measurements have been performed weighing and measuring the total volume of the samples. Large bar errors come, basically, from total volume measurements, which were obtained with the help of a microscope.

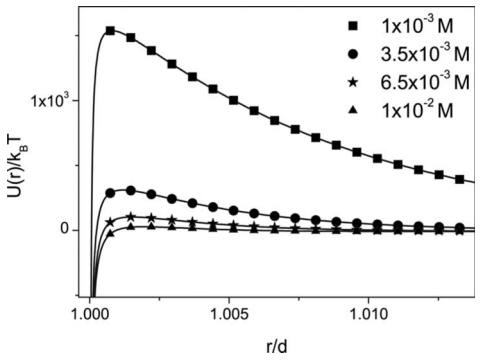

FIG. 4. Plot of two-body sphere-sphere potential $U(r)$ vs reduced distance r/d for different electrolyte concentrations. The total potential is relative to the thermal energy.

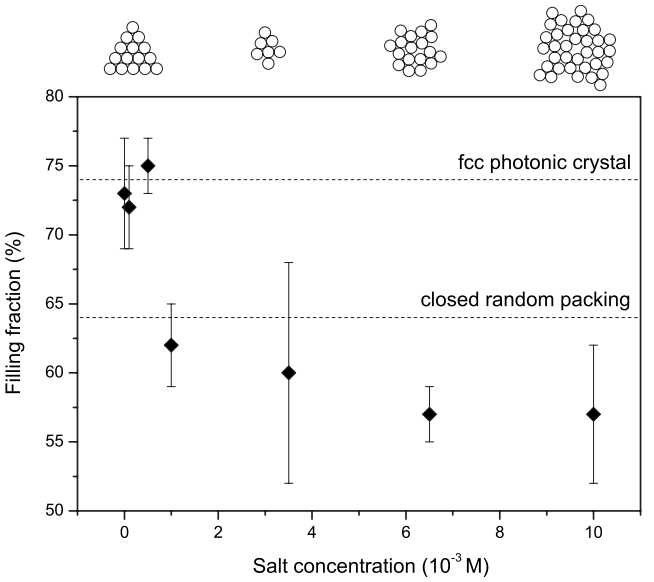

FIG. 5. Plot of the average ff of a photonic glass as a function of electrolyte (salt) concentration. Spheres that composed the glass are 1220 nm diam. Filling fraction can be estimated by weighting the samples when their geometry is known. A concentration 0 M gives rise to a well known opal-based photonic crystal where the total volume occupied by the spheres is 74% of the total volume of the unit cell in an fcc lattice.

III. DIFFUSE LIGHT TRANSPORT

A. Diffusion equation

When light travels through a PG it is multiply scattered. Straight or ballistic propagation, which is characteristic in a homogeneous medium, cannot describe accurately the transport of flight. We will briefly review here the standard diffusion model used to quantitatively describe light transport in an isotropic random dielectric medium. The multiple scattering of light has a very complicated solution in terms of Maxwell equations when many scatterers have to be taken into account. A model to solve this problem is the radiative transfer equation of the dilute medium where phase and light interference are neglected. The solution of the radiative transfer equation can be considerably simplified by introducing further approximations. The diffuse approximation considers a random walk of photons and imposes a continuity equation for the light intensity $I(\bar{r},t)$ disregarding interference effects. Propagation of light can, therefore, be viewed as a diffusion process such as gasses diffusing in a partial pressure gradient. The most important parameter is the scattering mean free path, ℓ_s, which is the average distance between two consecutive scattering events. This parameter sets the limits of the diffusive approximation as $\lambda \ll \ell_s \ll L$ (several scattering events occur before the light leaves the system, where L is the system size, hereafter sample thickness) and $k\ell_s \gg 1$ (limits the approximation to a dilute medium, where k is the light wave vector). After several scattering events, the light propagation is completely randomized. The transport mean free path, ℓ_t, is defined as the average distance after which the intensity distribution becomes isotropic and is the characteristic length in the regime of multiple scat-

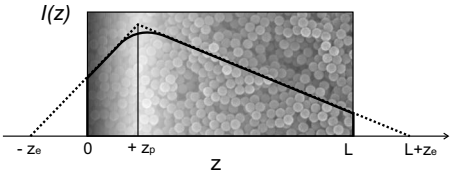

FIG. 6. Scheme of the light intensity vs distance into a slab of a photonic glass. Extrapolation length z_e and penetration length z_p are shown.

tering. The transport of ballistic or unscattered light in such a medium in space (r) and time (t) is dictated by the Lambert-Beer equation, $I(\bar{r},t)=I(0,t)\exp(-\bar{r}/\ell_s)$, while diffuse light propagates according to the diffusion equation as follows:

$$\left(\frac{\partial}{\partial t} - D\cdot\nabla^2 + \frac{\nu_e}{\ell_i}\right) I(\bar{r},t) = S(\bar{r},t). \tag{1}$$

$S(\bar{r},t)$ is the light source and v_e is the energy velocity. Multiple scattering increases the interaction between light and the system. When the material that composes the system presents absorption, its effect is increased in a diffusive propagation. The inelastic absorption length, ℓ_i, is the average depth at which light propagates ballistically (straightforward) in a homogeneous medium before being attenuated by a factor e. The diffusive absorption length, ℓ_a, is the distance light propagates diffusively before being absorbed. Inside a diffusive and absorbing material, ℓ_a is the penetration depth of the diffuse light. Diffuse light propagates a greater distance than in a homogeneous material to reach the same depth. For this, ℓ_a is shorter than ℓ_i. However, both are not independent functions but are related to ℓ_t as

$$\ell_a = \sqrt{(\ell_t \ell_i)/3}. \tag{2}$$

The experimental systems treated in this work have a slab geometry that imposes certain boundary conditions on the diffusion equation: the system can be considered infinite for x and y directions and limited between $z=0$ and $z=L$. An incident plane wave is originated at $z=-\infty$ and, due to multiple scattering, decays exponentially inside the system according to the Lambert-Beer equation. Dirichlet boundary conditions to the diffusion equation are

$$I(z)=0 \text{ at } \begin{cases} z=-z_{e1}, \\ z=L+z_{e2}, \end{cases} \tag{3}$$

where $z_{e1,2}$ are the extrapolation lengths, of the order of ℓ_s, which are the positions where the diffusive light intensity is zero and, eventually, can be different at the front and back surfaces (if their reflectivities are different). A common phenomenological way [24] to introduce a source is to consider an exponentially decaying one, $S(z)=S(0)\exp(-z/z_p)$, with a penetration length z_p. Figure 6 schematically reproduces a slab geometry system with the parameters related to the diffusion equation such as z_e and the penetration length z_p. These lengths are typically set to be identical $(z_e=z_p)$.

B. Stationary solution

The stationary solution of the diffusion equation leads to the total transmission of light through a photonic glass slab given by [25]

$$T(L,\lambda) = \frac{1}{\alpha z_e}\frac{\sinh[\alpha(z_p+z_e)]\sinh[\alpha z_e]}{\sinh[\alpha(L+2z_e)]},$$

$$z_e = \frac{1}{2\alpha}\ln\left(\frac{1+\alpha z_0}{1-\alpha z_0}\right),$$

$$z_0 = \frac{2}{3}\ell_t(\lambda)\left(\frac{1+R}{1-R}\right). \tag{4}$$

In the solution, $\alpha=1/\ell_i$ is the inverse absorption length and R is the polarization and angular averaged reflectivities of the boundaries [26]. As in electronic transport and in the absence of absorption, doubling the thickness of the (optical) conductor halves the transmission. This is known as photonic Ohm's law. The diffusion of light in a disordered dielectric slab and, in particular, a photonic glass leads to the photonic Ohm's law. The total light transmission through a photonic glass slab is directly proportional to the transport mean free path, ℓ_t, and inversely proportional to the slab thickness, $T(\lambda) \sim \ell_t(\lambda)/L$. Therefore, with static measurements of the total light transmission through a slab with known thickness, it is possible to obtain the absolute value of the transport mean free path, ℓ_t.

C. Full time-dependent solution

The full solution of the time-dependent diffusion equation with boundary conditions is given by [27]

$$T(t,\lambda) = \frac{\exp(-t/\tau_i)}{4t(4\pi t D(\lambda))^{3/2}}\left(\sum_{j=-\infty}^{+\infty} A\exp[-A^2/4D(\lambda)t] - \sum_{j=-\infty}^{+\infty} B\exp[-B^2/4D(\lambda)t]\right),$$

$$A = (1-2j)(L+2z_e) - 2(z_p+\ell_t),$$

$$B = (2j+1)(L+2z_e),$$

$$\tau_i = \frac{\ell_i^2}{D},$$

$$z_e = \frac{1}{2\alpha}\ln\left(\frac{1+\alpha z_0}{1-\alpha z_0}\right),$$

$$z_0 = \frac{2}{3}\ell_t(\lambda)\left(\frac{1+R}{1-R}\right), \tag{5}$$

where the inelastic absorption length, $\ell_i(\lambda)$, turns into an absorption or inelastic time $\tau_i(\lambda)$. The rate of diffuse light transport in the photonic glass is defined by the diffusion constant, D, given by Fick's law [28]. This is, therefore, a

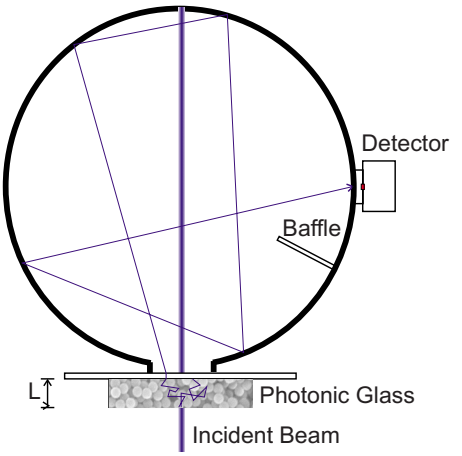

FIG. 7. (Color online) Cartoon of the experimental setup to perform static measurements. A slab of photonic glass with thickness L is placed in the entrance of an integrating sphere and illuminated with white light. Diffuse light is measured in the detector.

dynamic variable, and a time-resolved measurement of light transmission is needed to obtain its value. The physical meaning of the summatory in Eq. (5) can be understood as follows: light that follows shorter optical paths thought the slab is transmitted at earlier times, while light that performs longer random walks emerges at much longer times. The total transmission is therefore given by the sum of all these contributions. This produces a time spread of the initial pulse, which depends on the diffusion constant. The behavior at long time is dominated by the least decaying exponential, giving the time tail decay rate $\tau_d = \pi^2 D/(L+z_{e1}+z_{e2})$.

IV. STATIC MEASUREMENTS

Figure 7 schematically sketches the set up used to perform static measurements: an integrating sphere that consists of a hollow cavity with its interior coated for high diffuse reflectance. Photonic glasses slabs with different thicknesses are placed on the integrating sphere entrance hole. White light from a tungsten lamp is sent into the sample. The integrating sphere placed after the sample collects all the light exiting at all angles, and sends it to a fiber coupled miniature spectrometer that allows resolving the various spectral contributions with a sub-nm resolution. The sample is optically very thick; therefore, ballistic or unscattered light propagating through it is exponentially attenuated. We can therefore assume that only diffusive light comes out at any angle from the sample and enters the integrating sphere. Figure 8 shows a direct measurement of the total diffused light transmission through different photonic glass slabs (thickness $L \sim 100\ \mu$m) upon white light illumination in the range 500–920 nm. In order to be able to compare the optical response of different sphere sizes (790, 930, 1000, and 1220 nm), we plot the measurements as a function of reduced units (dn/λ), where n is the refractive index.

Oscillations in transmission and its spectral dependence are due to the existence of modes for the electromagnetic field in the spheres. The spectral positions of these Mie

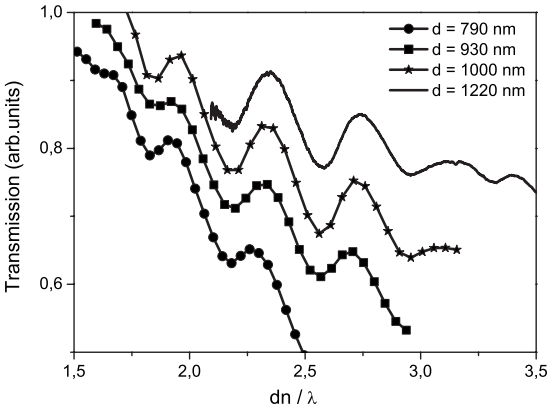

FIG. 8. Normalized total transmission of white light through photonic glasses as a function of the reduced parameter dn/λ. Samples are composed by spheres with four different diameters, and thickness is about 100 μm in all cases.

modes depend exclusively on sphere diameter, d, and on its refractive index, n. These electromagnetic modes are excited when the electromagnetic field wavelength is comparable with the optical diameter of the spheres.

Figure 8 shows clear and simple evidence of the resonant behavior of light transport in a broad energy interval. In order to demonstrate this fact and also to clarify the conditions under which the modes can be collectively excited, we compared the resonant behavior of these four different sphere sizes with two different no-resonant dielectric random systems. Figure 9 plots the total transmission through two reference samples that, for two different reasons, do not exhibit resonant behavior. As Fig. 9 points out, there is no trace of resonances in the transport of light for these two reference systems. The first one (dashed curve) is a photonic glass composed by PS spheres with a diameter of 200 nm. The

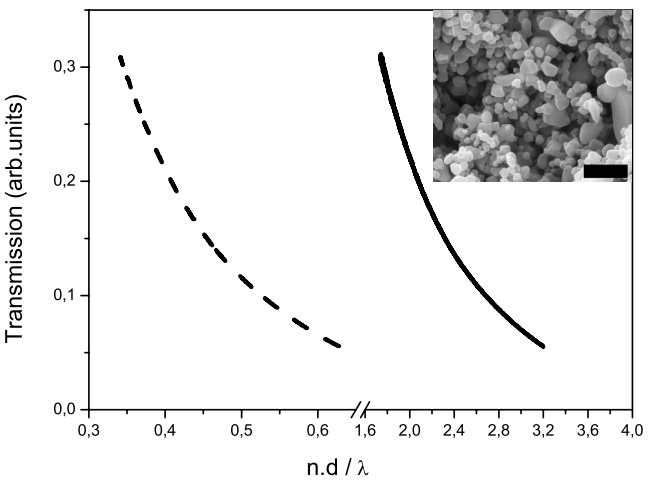

FIG. 9. Total transmission of white light through two different reference samples as a function of the reduced parameter dn/λ. The dashed line represents total transmission through a photonic glass made of PS spheres of $d=200$ nm. Solid line represents total transmission through polydisperse TiO_2 of averaged $d=850$ nm (SEM inset of the sample where the scale bar represents 200 nm). Both present nonresonant light transmission.

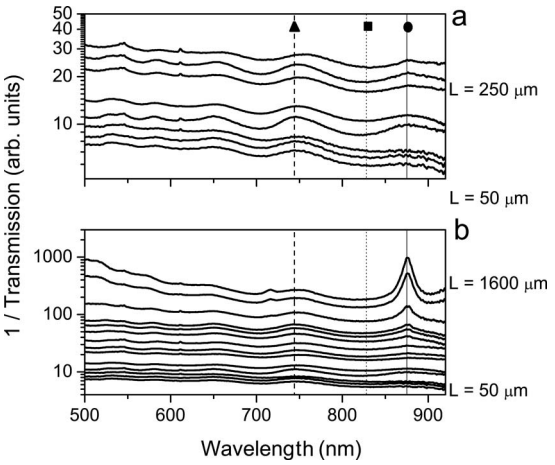

FIG. 10. Inverse of total light transmission of white light through photonic glasses made of PS spheres with $d=1220$ nm as a function of wavelength. (a) For low values of L ($\ell_a > L$). In this case, thicknesses vary from 50 to 250 μm. (b) For high values of L ($\ell_a < L$), up to 1600 μm, transmission shows a linear dependence on thickness except for those wavelengths where absorption is not negligible. Three particular wavelengths are marked with a triangle ($\lambda_1=744$ nm), a square ($\lambda_2=828$ nm), and a circle ($\lambda_3=875$ nm).

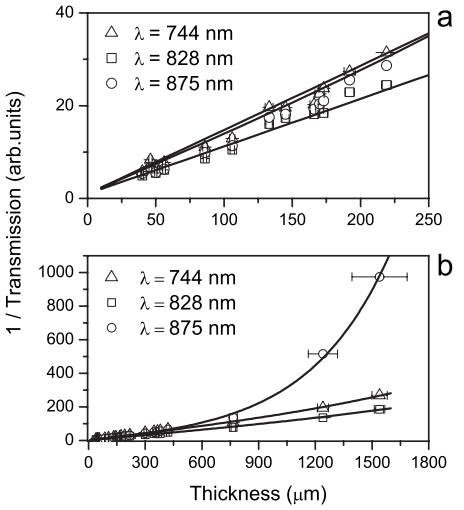

FIG. 11. Plot of T^{-1} as a function of the thickness for three different wavelengths. (a) For low $L(\ell_a \gg L)$, linear dependence is clearly shown for $\lambda=744$, 828 and 875 nm as an indication of the validity of the Ohm's law for this wavelengths which present, however, different slopes. (b) For high L ($\ell_a < L$), exponential behavior is revealed for $\lambda=875$ nm related to a water absorption.

small size of the spheres compared to the light wavelength illumination ($dn/\lambda \sim 0.4$ does not allow them to sustain Mie modes in the wavelength range where the measurements are performed. Therefore, those spheres behave, upon this particular light energy illumination, as pointlike scatters giving rise to Rayleigh scattering (where scatter structure is negligible) instead of Mie scattering (where resonances can be sustained). Resonances are expected in other energy ranges (in the uv) for this particular system. The second one (solid curve) is composed of TiO_2 nonspherical powders with a polydispersity about 36% (see the inset of Fig. 9) and a mean diameter of about 850 nm. A different situation comes with the nonresonant light transport through TiO_2 powder. In this case, TiO_2 particles are large enough ($dn/\lambda \sim 2.5$) to sustain Mie modes in this wavelength interval. However, Fig. 9 shows no trace of oscillations in the light transport because resonances are smoothed out by polydispersity and the arbitrary nonspherical shape of the scatters. As previously remarked, Mie modes are morphologically defined by the geometry of the scatterer. When the scatterers are nonspherical and also polydisperse, as in the TiO_2 case, each building block sustains resonances for different wavelengths. This smooths out the collective response giving rise to an overall nonresonant behavior.

A. Resonant mean free path

In order to completely characterize these systems, total transmission, $T(L,\lambda)$, was measured as a function of the slab thickness (L, from 50 to 1600 μm) for a fixed sphere diameter ($d=1220$ nm) and at extended wavelength range ($500 < \lambda < 920$ nm), which $T(L,\lambda)^{-1}$ is shown in Fig. 10. From the experiments, it is possible to fit the values of $\ell_t(\lambda)$, the transport mean free path, and $\ell_a(\lambda)$, the absorption length. When light propagates diffusively and in the absence of absorption ($\ell_a \gg L$), the function $1/T(L,\lambda)$ is directly proportional to the slab thickness, L [Fig. 11(a)]. From this set of samples, represented in Fig. 10(a), we can obtain $\ell_t(\lambda)$ by fitting the experimental results with the stationary solution of the diffusion Eq. (4). Figure 12 shows this fit for the extended wavelength range. It reveals a clear resonant behavior of $\ell_t(\lambda)$. In the curve, a triangle and a square mark the spectral positions of a minimum and a maximum of $\ell_t(\lambda)$, respectively.

The scattering cross section is enhanced when a Mie mode is excited in a sphere. The scattering is more efficient at those wavelengths and, therefore, the transport mean free path becomes minimum.

B. Absorption

Absorption provokes an exponential dependence of $1/T(L,\lambda)$ on the slab thickness [pointed out in Fig. 10(b)]

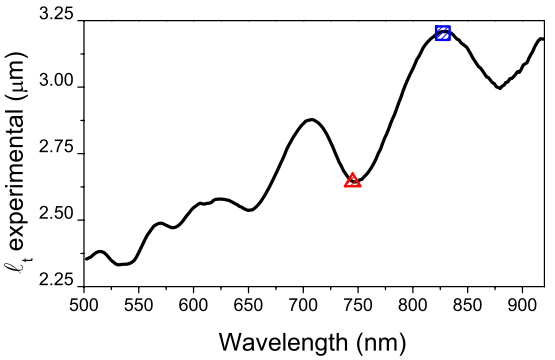

FIG. 12. (Color online) Experimental transport mean free path in a photonic glass made of PS spheres of $d=1220$ nm. The data are obtained by fitting experimental T^{-1} curves. Two particular wavelengths are marked with a triangle ($\lambda_1=744$ nm), a square ($\lambda_2=828$ nm).

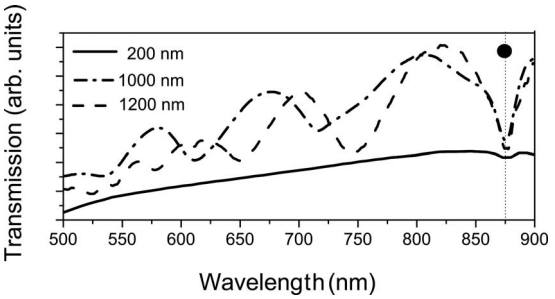

FIG. 13. Total white light transmission through photonic glasses composed by PS spheres with 200 nm (straight line), 1000 nm (dashed-dot line) and 1200 nm (dashed line) as a function of wavelength. All the spectra present a peak absorption at $\lambda=875$ nm (marked with a circle) related to water.

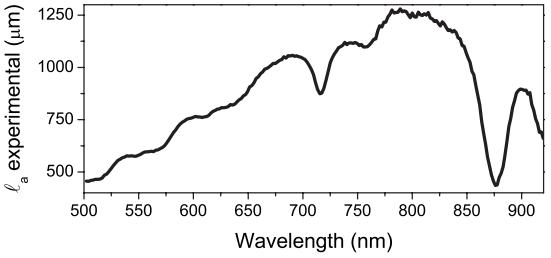

FIG. 14. Plot of the absorption length, ℓ_a, from a photonic glass made of PS with $d=1220$ nm. It shows clearly two absorption peaks at $\lambda=875$ nm, $\lambda=730$ nm related to liquid water absorptions.

and must be carefully characterized. Figure 11(b) plots the value of $1/T(L,\lambda)$ as a function of slab thickness (L) at three particular wavelengths, which have been previously marked in Fig. 10 with a triangle ($\lambda_1=744$ nm), a square ($\lambda_2=828$ nm), and a circle ($\lambda_3=875$ nm). In the first and second cases, $\lambda_1=744$ nm and $\lambda_2=828$ nm, the function $1/T(L,\lambda)$ presents a linear dependence on L, while in the third case, $\lambda_3=875$ nm, it presents an exponential dependence.

Wavelengths λ_1 and λ_2 correspond to a minimum and a maximum of a Mie resonance, respectively. The different slopes agree with the photonic Ohm's law with negligible absorption $[\ell_a(\lambda_1,\lambda_2)>L]$ and different ℓ_s. Contrary to these cases and when L is large enough, a clear absorption peak is revealed at wavelength λ_3. This can be easily seen in Fig. 10(b) and is made more apparent in Fig. 11(b), where the function $1/T(L,\lambda)$ presents a clear exponential dependence on L.

In order to clarify and distinguish Mie resonances from absorption peaks, the same transmission experiments have been performed for different sphere diameters. Figure 13 shows the total light transmission through three particular photonic glass slabs composed of different sphere sizes with diameters 200, 1000, and 1200 nm, respectively. These slabs are thick enough to present the peak absorption at $\lambda_3=875$ nm. Therefore, $\ell_a(875\text{ nm})<L$ in all these cases. This peak is independent of the sphere diameter and, for this reason, it cannot originate from a Mie resonance, which only depends on the geometric parameters of the scatterers. In addition, as a photonic glass slab composed of spheres with $d=200$ nm cannot sustain collective Mie resonances, we deduce, that the peak must be due to a discrete absorption. We show that, for certain wavelengths, the system presents discrete absorptions that are revealed in optical spectroscopic measurements only when $\ell_a<L$. At this point, it is necessary to estimate the value of this diffusive length in the energy range at which experiments have been performed. Figure 14 shows the diffusive absorption length, $\ell_a(\lambda)$, obtained by fitting the experimental curve of the function $1/T(L,\lambda)$ with the corresponding Eq. (4). Valuable information is revealed in this plot: (i) the mean value of the absorption length (ℓ_a) is about 1 mm; (ii) two dips at wavelengths $\lambda=730$ and 875 nm appear in the function $\ell_a(\lambda)$, for which ℓ_a presents values about 900 and 500 μm, respectively, and, consequently, absorption is maximum; (iii) an uv absorption tail is pointed out at higher energies (lower wavelengths), where ℓ_a presents a continuous decay. The exponential dependence of the function $1/T(L,\lambda)$ on L at high energies is related to uv PS absorption [29].

At lower energies, the material that composed the spheres (PS) has no absorption [29]. According to this, we attribute the peaks at $\lambda=730$ and 875 nm to near-infrared states of residual liquid water in the sample due to overtones and combination bands of fundamental vibrations occurring in the midinfrared [30]. To rule out other possible effects of the salt used to destabilize the colloidal suspension, we have grown different photonic glasses varying the growth conditions. As mentioned in the preceding section, an extra amount of charge is enough to attenuate the electrostatic potential into a total attractive potential. This extra amount of charge can be obtained by adding salts (ionic or covalent) or acids as both, when in dissolution, dissociate producing ions or electrolytes. To verify that no discrete absorption peaks were due to salt, we have grown photonic glasses with different kinds of salts ($CaCl_2$, NaCl, K_2CO_3, $MgSO_4$, and Na_2CO_3) and also with acid (HCl). Their optical response is always the same and shows the same absorption peaks, which, therefore, cannot be due to the salt nor PS.

A short comment about absorption in photonic glasses compared to other photonic systems is needed. As previously settled, light transport through highly disordered materials is diffusive in opposition to ballistic or unscattered transport through nondiffusive materials. Although absorption disturbs the optical properties of all photonic systems, its effects are more evident in diffusive materials. Opal-based photonic crystal is a paradigmatic system where light transport is, in principle, ballistic in spite of being grown with the same building blocks as a photonic glass. Absorption effects that can be neglected or unobservable, for example in a photonic crystal, should be taken into account and carefully characterized in photonic glasses. This fact is explained attending to the different light transport properties that take place in each one. In a diffusive material, the characteristic absorption length is ℓ_a, whereas in a nondiffusive material absorption is characterized with the length ℓ_i, which is the distance that light travels before being attenuated a factor e. According to Eq. (2), ℓ_i is always longer than ℓ_a and, therefore, light should propagate a much longer ballistic distance in photonic crystal to become attenuated with the same factor as in a photonic glass.

We can do an estimation of the main values of both ℓ_a and ℓ_t, and also the main value of ℓ_i. At the wavelengths for

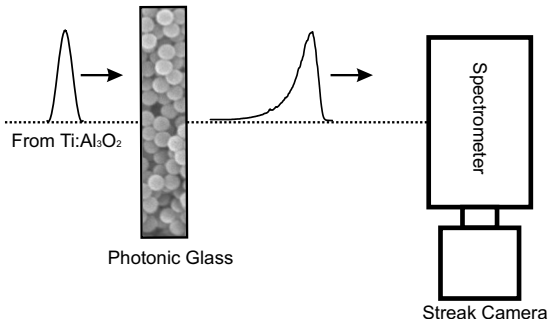

FIG. 15. Experimental set up to perform dynamical measurements. A ultrashort laser pulse is sent to the sample. A spectrometer collects the pulse temporally spreaded by the sample and sends it to a streak camera.

which peak absorptions have been observed, a value of $\ell_a \sim 800\ \mu$m gives rise to $\ell_i \sim 0.7$ m (with a value of $\ell_t \sim 3\ \mu$m). It is remarkable the big difference (three orders of magnitude) between the absorption length (ℓ_i) and the diffusive absorption length (ℓ_a). This fact suggests that, to observe the same absorption effects in a pass-band photonic crystal, it should be necessary to build a photonic crystal 1000 times thicker than a photonic glass, that is, 1 m thicker.

V. DYNAMIC MEASUREMENTS

Once the static photonic properties of photonic glasses have been examined, we are interested in the dynamic transport parameters. In the experimental setup to perform a time-resolved measurement (schematically shown in Fig. 15), we use a streak camera that permits us to monitor the time evolution of a very short laser pulse in its propagation through the glass. In particular, we have performed the experiment with 2 ps pulses provided by a $Ti:Al_2O_3$ laser tuneable within 700–920 nm. An example of a time-resolved transmission measurement is plotted in Fig. 16 for two different

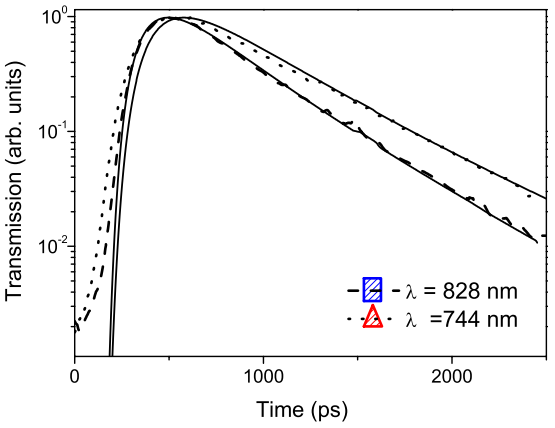

FIG. 16. (Color online) Time-resolved transmission measurements at $\lambda = 744$ and 828 nm where the different slope of $T(t)$ gives rise to a minimum [$D(744) = 166\ m^2/s$] and a maximum [$D(828) = 205\ m^2/s$] in the diffusion constant. In this case, $L = 1120\ \mu$m. (Straight lines represent the fit of the experimental measurements with the diffusion equation.)

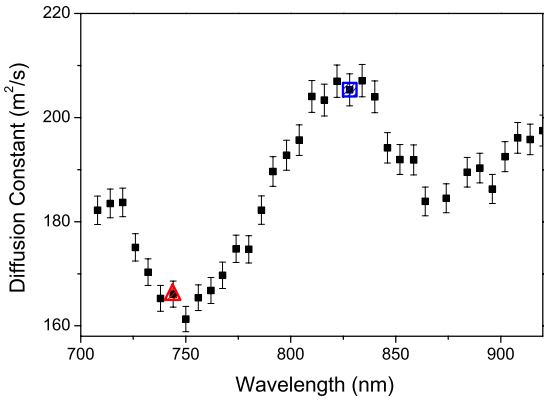

FIG. 17. (Color online) Experimental diffusion constant in a photonic glass made of PS spheres with $d = 1220$ nm obtained by fitting experimental $T(t)$ curves. Two particular wavelengths are marked with a triangle ($\lambda_1 = 744$ nm) and a square ($\lambda_2 = 828$ nm).

wavelengths, $\lambda_1 = 744$ nm and $\lambda_2 = 828$ nm, which correspond to the minimum and the maximum of a Mie resonance analyzed in the preceding section. The different slope of $T(t,\lambda)$ at long times (the time decay) at these two different wavelengths accounts for the presence of a Mie resonance. The thickness of the photonic glasses used in these time-resolved experiments is about 1 mm. Figure 17 evidences the resonant behavior of $D(\lambda)$. Its value has been obtained fitting the experimental time profile of $T(t,\lambda)$ with the dynamical solution of the diffusion equation (5). The solution to the diffusion equation, with appropriate boundary conditions, fits well the experimental data. The value of $\ell_a(\lambda)$ has been obtained independently from static measurements, using Ohm's law, and can be introduced in the equation as a known parameter.

This provides an accurate estimation of the value of $D(\lambda)$. Absorption accounts for a correction of only a few %, on average, but is crucial on the absorption peak (at $\lambda = 875$). We can conclude that the resonant behavior of $D(\lambda)$ is due to Mie modes and presents maxima and minima at the same spectral positions as in the static measurements of $\ell_t(\lambda)$.

VI. DISCUSSION

The appropriate velocity that describes light diffusive transport in photonic glasses is the energy velocity. A discussion about the possible resonant behavior of this magnitude can be found in the literature [9,31,32]. Figure 18 represents the energy velocity, v_E, obtained from independent measurements of $\ell_t(\lambda)$ (static) and $D(\lambda)$ (dynamic) with the help of the expression

$$\mathcal{D} = \tfrac{1}{3} v_E \ell_t. \tag{8}$$

The experimental value is below the average value of the group velocity obtained from the sample average refractive index $v_g = c/\langle n \rangle \sim 0.77c$ while showing clear resonances. Qualitatively, the minima of $\ell_t(\lambda)$, for which the scattering strength is maximum, correspond to wavelengths that excite a Mie mode, and therefore experience a longer dwell time. This turns into a minimum transport velocity (Fig. 18). For

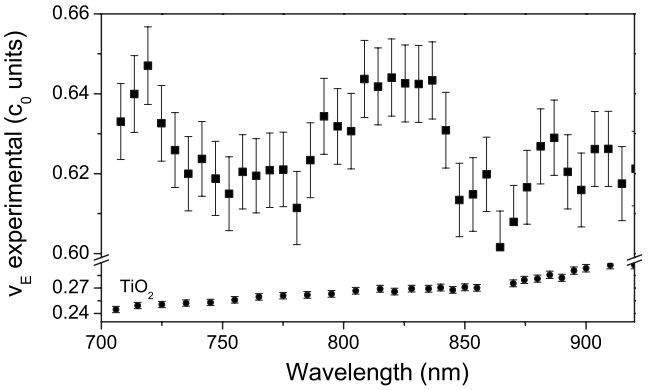

FIG. 18. Experimental values of the energy velocity as a function of the wavelength for a photonic glass made of PS sphere with diameter $d=1220$ nm and for TiO_2 powder. For the photonic glass, a full oscillation of around 5% amplitude is shown. The averaged medium group velocity is $0.77c$. For the TiO_2 powder, flat velocity dispersion is shown, obtained with the same procedure (note the different scales on the y axis).

comparison, we show at the bottom of Fig. 18 the lack of velocity dispersion of a TiO_2 powder sample measured in the same experimental conditions. For ideal microspheres, the single-particle resonances are 10–20 % wide in wavelength, and therefore they are expected to be washed out for ff $>5-10$ % (see the lower curve in Fig. 18). Recently, Stoerzer *et al.* [11] reported a wavelength-dependent diffusion constant in 15–20 % polydisperse, irregularly shaped titania powders, which in light of our findings is unlikely to be the result of Mie resonances. The importance of the morphology of the sphere is evident, as a broad size distribution or a random shape of the dielectric resonator are expected to wash out the resonant properties [33,34].

Figure 19 shows the comparison between the experimental and theoretical plots of $\ell_t(\lambda)$ obtained by analytically solving the Mie modes in a single dielectric sphere. This theory can be rigorously applied to the single scattering regime or, in the case of diluted systems, to independent scattering events. The partial disagreement between experimental and theoretical data comes from the fact that our system cannot be considered diluted with a filling fraction of 0.55. When the scatterer density is very low, a multiple scattering theory with a single scatter t-matrix appropriates [10]. This holds roughly until the optical (and not physical) sizes of the scatterers start to overlap. Then, the modes start to interact and should affect the scattering matrix of the sphere. Finally, it is expected that the resonances will disappear when the scatterers occupy a volume fraction of 100%. The coherent-potential approximation [32], which is a mean-field theory and a first order in scattering density, predicts that the scattering resonances weaken at high ffs and even disappear for ff $\sim 50-60$ %. Nevertheless, at a filling fraction as high as 0.55, it is still possible to experimentally resolve the effect of Mie resonances in the transport mean free path and transport velocity, as we show. It is interesting to look further into the physics involved in the resonant behavior at intermediate filling fractions. When optimizing light diffusion, one often wants to increase the refractive index contrast and to maximize the scatterers density in order to minimize the scattering mean free path. The price to be paid when increasing the ff is to induce both correlations in the scatterers' relative positions (in the close-packing limit, only the crystalline fcc lattice is allowed) and interaction between the Mie modes inside scatterers. As long as the suspensions are dilute, the scatterers can be considered independent and intraparticle scattering [represented by the form factor $F(q)$] is sufficient to describe the system.

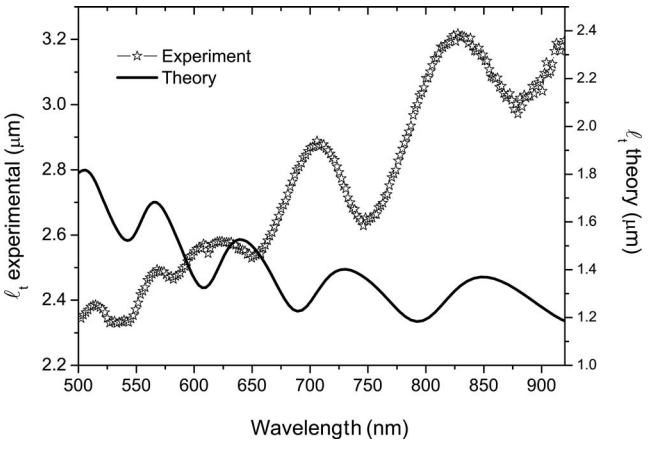

FIG. 19. Plot of the transport mean free path: experimental (stars), theoretical prediction of single-sphere Mie theory [9] for ideal spheres (straight line).

If the concentration increases, however, in addition to intraparticle scattering, interparticle scattering [represented by the structure factor $S(q)$] must be taken into consideration. The relation between transport mean free path and the microscopic scattering properties is given by [27,35]

$$\frac{1}{\ell_t} = \frac{\pi}{k^6}\int_0^{2k} \rho F(q) S(q) q^3 dq, \tag{9}$$

where ρ is the number density and q the single-scattering wave vector. One can work with a modified structure factor, $S(q)$, in order to fit the data [36] or confront a new calculation of $F(q)$ taking into account the possible interactions between the modes of a sphere and near neighbors.

Figure 20 shows the comparison between experiment, single sphere theory, and the calculation of $S(q)$ obtained in the Percus-Yevick approximation for hard spheres [37]. It evidences how $S(q)$ alone cannot account for the resonances that appear in the transmission spectrum. A solution to this problem is, in our opinion, a multiple scattering theory with a modified single scatterer $F(q)$ that takes into account the possible interactions with nearest neighbors. Effectively, the point is to calculate an adequate $F(q)$ that accounts accurately for the strength of the resonances. Finally, polydispersity and refractive index contrast of the structure are important in determining the visibility of the resonances. Figure 21 shows the plot of ℓ_t simulated for four different values of sphere polydispersity and two different values of sphere refractive index corresponding to PS and silicon. It shows how, increasing the polydispersity, the resonances are washed out. Even in the case of a high refractive index contrast, a poly-

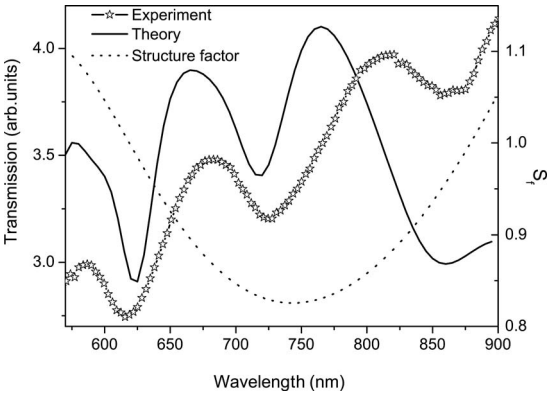

FIG. 20. Experimental (stars) and theoretical (straight line) transmission from a PG with spheres $d=550$ nm. The dotted line shows the calculated structure factor $S(q)$.

dispersity of 5% is enough to smooth all the main spectral features. This theoretical prediction agrees with our measurements, which show how a high polydispersity gives rise to nonresonant light transport (Fig. 9) even in the case of high refractive index contrast, as in the case of TiO_2.

VII. CONCLUSIONS

In conclusion, we present an ample optical characterization of photonic glasses. With independent experiments (static and dynamic), we observe resonant behavior in diffuse light transport: resonant transport mean free path, diffusion constant, and energy velocity. This observation opens new and encouraging routes in the field of light transport through disorder media as photonic glasses can be powerful systems to be used as a new playground for light diffusion. This novel material joins light dispersion and diffusion in the same system, a combination that can be crucial to control the

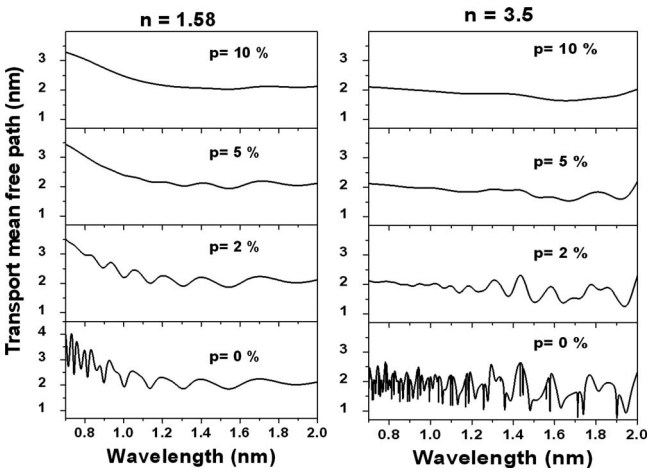

FIG. 21. Analytical calculations of the transport mean free path for four values of sphere polidispersity, p, and for two different values of sphere refractive index. Sphere diameters are 1 μm and ff=0.5.

diffuse flow of light in analogy to what photonic crystals do for ballistic light. For example, phenomena such as Anderson localization of light or random lasing in combination with resonances in $\ell_t(\lambda)$ acquire promising possibilities in this novel framework. Photonic glasses by themselves and integrated with photonic crystals may give rise to new applications in future photonic devices.

ACKNOWLEDGMENTS

The work was supported by the EU through Network of Excellence IST-2-511616-NOE (PHOREMOST), CICyT NAN2004-08843-C05 and 09109–C04, MAT2005–01388, and MAT2006-09062, the Spanish MEC Consolider-QOIT CSD2006-0019, and the Comunidad de Madrid S-0505/ESP-0200. Á.B. and M.D.M. also thank the R&C program.

[1] P. Sheng, *Introduction to Wave Scattering, Localization, and Mesoscopic Phenomena* (Academic, San Diego, 1995).
[2] E. Yablonovitch, Phys. Rev. Lett. **58**, 2059 (1987).
[3] S. John, Phys. Rev. Lett. **58**, 2486 (1987), P. W. Anderson, Philos. Mag. B **52**, 505 (1985).
[4] Y. Kuga and A. Ishimaru, J. Opt. Soc. Am. A **8**, 831 (1984); M. P. Van Albada and A. Lagendijk, Phys. Rev. Lett. **55**, 2692 (1985); P. E. Wolf and G. Maret, *ibid.* **55**, 2696 (1985).
[5] S. Fraden and G. Maret, Phys. Rev. Lett. **65**, 512 (1990); M. P. van Albada, J. F. de Boer, and A. Lagendijk, *ibid.* **64**, 2787 (1990); P. Sebbah, B. Hu, A. Z. Genack, R. Pnini, B. Shapiro, *ibid.* **88**, 123901 (2002).
[6] F. Scheffold and G. Maret, Phys. Rev. Lett. **81**, 5800 (1998).
[7] L. F. Rojas-Ochoa, J. M. Mendez-Alcaraz, J. J. Saenz, P. Schurtenberger, and F. Scheffold, Phys. Rev. Lett. **93**, 073903 (2004).
[8] Ad Lagendijk and B. van Tiggelen, Phys. Rep. **270**, 143 (1996).
[9] M. P. van Albada, B. A. van Tiggelen, A. Lagendijk, and A. Tip, Phys. Rev. Lett. **66**, 3132 (1991).
[10] G. Labeyrie, E. Vaujour, C. A. Muller, D. Delande, C. Miniatura, D. Wilkowski, and R. Kaiser, Phys. Rev. Lett. **91**, 223904 (2003).
[11] M. Storzer, C. M. Aegerter, and G. Maret, Phys. Rev. E **73**, 065602(R) (2006).
[12] D. S. Wiersma, P. Bartolini A. Lagendijk, and R. Righini, Nature **390**, 671 (1997).
[13] X. H. Wu, A. Yamilov, H. Noh, H. Cao, E. W. Seelig, and R. P. H. Chang, J. Opt. Soc. Am. B **21**, 159 (2004).
[14] N. Garcia and A. Z. Genack, Phys. Rev. Lett. **66**, 1850 (1991).
[15] P. M. Johnson, A. Imhof, B. P. J. Bret, J. G. Rivas, and A. Lagendijk, Phys. Rev. E **68**, 016604 (2003).
[16] These optical modes are confined by continuous total internal reflection at the dielectric air interface and are often referred to as whispering-gallery modes. This description originated from the "problem of the whispering-gallery" which Lord Rayleigh published in 1912, Scientific Papers 5:617, describing the phenomenon of acoustical waves he had observed propagating

around the interior gallery of Saint Paul's Cathedral. Anyhow, Maxwell equations can be solved exactly for the spherical scatterer: G. Mie, Ann. Phys. **25**, 377 (1908).
[17] Simulations were performed with meep [A. Farjadpour, D. Roundy, A. Rodriguez, M. Ibanescu, P. Bermel, J. D. Joannopoulos, S. G. Johnson, and G. Burr, Opt. Lett. **31**, 2972 (2006)].
[18] M. I. Antonoyiannakis and R. Pendry, Europhys. Lett. **40**, 613 (1997).
[19] P. D. Garcia, R. Sapienza, A. Blanco, and C. Lopez, Adv. Mater. (Weinheim, Ger.) **19**, 2597 (2007).
[20] R. Sapienza, P. D. Garcia, J. Bertolotti, M. D. Martin, A. Blanco, L. Vina, C. Lopez, and D. S. Wiersma, Phys. Rev. Lett. **99**, 233902 (2007).
[21] P. Jiang, J. F. Bertone, K. S. Hwang, and V. L. Colvin, Chem. Mater. **11**, 2132 (1999).
[22] K. L. Wu and S. K. Lai, Langmuir **21**, 3238 (2005).
[23] Filling fraction ff is defined as the volume occupied by the spheres divided by the total volume of the system.
[24] D. J. Durian, Appl. Opt. **34**, 7100 (1995).
[25] N. Garcia, A. Z. Genack, and A. A. Lisyansky, Phys. Rev. B **46**, 14475 (1992).
[26] J. X. Zhu, D. J. Pine, and D. A. Weitz, Phys. Rev. A **44**, 3948 (1991).
[27] M. S. Patterson, B. Chance, and B. C. Wilson, Appl. Opt. **28**, 2331 (1989).
[28] A. Fick, Ann. Phys. Chem. **94**, 59 (1855).
[29] T. Inagaki, E. T. Arakawa, R. N. Hamm, and M. W. Williams, Phys. Rev. B **15**, 3243 (1977).
[30] J. A. Curcio and C. C. Petty, J. Opt. Soc. Am. **41**, 302 (1951).
[31] C. M. Soukoulis, S. Datta, and E. N. Economou, Phys. Rev. B **49**, 3800 (1994).
[32] K. Busch and C. M. Soukoulis, Phys. Rev. B **54**, 893 (1996).
[33] S. C. Hill and R. E. Benner, "*Morphology-dependent resonances*," in *Optical Effects Associated with Small Particles*, edited by P. W. Barber and R. K. Chang (World Scientific, Singapore, 1988).
[34] G. H. Watson, P. A. Fleury, and S. L. McCall, Phys. Rev. Lett. **58**, 945 (1987).
[35] S. Fraden and G. Maret, Phys. Rev. Lett. **65**, 512 (1990).
[36] M. Reufer, L. F. Rojas-Ochoa, S. Eiden, J. J. Saenz, and F. Scheffold, Appl. Phys. Lett. **91**, 171904 (2007).
[37] L. Tsang, J. A. Kong, K. H. Ding, and C. O. Ao, *Scattering of Electromagnetic Waves: Numerical Simulations* (Wiley, New York, 2001).